

A FINITE ELEMENT VARIATIONAL MULTISCALE METHOD FOR THE NAVIER–STOKES EQUATIONS*

VOLKER JOHN[†] AND SONGUL KAYA[‡]

Abstract. This paper presents a variational multiscale method (VMS) for the incompressible Navier–Stokes equations which is defined by a large scale space L^H for the velocity deformation tensor and a turbulent viscosity ν_T . The connection of this method to the standard formulation of a VMS is explained. The conditions on L^H under which the VMS can be implemented easily and efficiently into an existing finite element code for solving the Navier–Stokes equations are studied. Numerical tests with the Smagorinsky large eddy simulation model for ν_T are presented.

Key words. variational multiscale method, finite element method, Navier–Stokes equations, turbulent flows

AMS subject classifications. 65M60, 76F65

DOI. 10.1137/030601533

1. Introduction. The flow of an incompressible fluid is governed by the incompressible Navier–Stokes equations

$$(1.1) \quad \begin{aligned} \mathbf{u}_t - \nu \Delta \mathbf{u} + (\mathbf{u} \cdot \nabla) \mathbf{u} + \nabla p &= \mathbf{f} && \text{in } (0, T] \times \Omega, \\ \nabla \cdot \mathbf{u} &= 0 && \text{in } [0, T] \times \Omega, \\ \mathbf{u} &= \mathbf{0} && \text{in } [0, T] \times \partial\Omega, \\ \mathbf{u}(0, \mathbf{x}) &= \mathbf{u}_0 && \text{in } \Omega, \\ \int_{\Omega} p \, d\mathbf{x} &= 0, && \text{in } (0, T]. \end{aligned}$$

Here, $\Omega \subset \mathbb{R}^d$, $d \in \{2, 3\}$, is a bounded domain with boundary $\partial\Omega$, $[0, T]$ a finite time interval, $\mathbf{u}(t, \mathbf{x})$ the fluid velocity, and $p(t, \mathbf{x})$ the fluid pressure. The parameters in (1.1) are the viscosity $\nu > 0$, which is inverse proportional to the Reynolds number $Re = \mathcal{O}(\nu^{-1})$, the prescribed body forces $\mathbf{f}(t, \mathbf{x})$, and the initial velocity field $\mathbf{u}_0(\mathbf{x})$.

Turbulent flows are characterized by a high Reynolds number. Due to the richness of scales in such flows, it is not possible to simulate them by a direct discretization of (1.1), e.g., by a Galerkin finite element method. The use of a turbulence model becomes necessary.

A currently very popular approach of turbulence modeling is large eddy simulation (LES). In LES, one seeks to simulate only the large scales of a turbulent flow accurately. This makes sense in applications, e.g., the prediction of a hurricane requires above all an accurate prediction of the few large eddies and not of the millions of small eddies. In classical LES, the large scales are defined by an averaging in space. However, this definition leads to serious problems if the flow is given in a bounded domain, which is the most frequent case in applications. Already the first step of deriving equations for the large scales introduces additional terms, so-called

*Received by the editors October 30, 2003; accepted for publication (in revised form) July 20, 2004; published electronically April 19, 2005.

<http://www.siam.org/journals/sisc/26-5/60153.html>

[†]Faculty of Mathematics, Otto-von-Guericke-University, Postfach 4120, 39016 Magdeburg, Germany (john@mathematik.uni-magdeburg.de).

[‡]Department of Mathematics, Illinois Institute of Technology, Chicago, IL 60616 (kaya@iit.edu). This author's work was partially supported by NSF grants DMS9972622, DMS20207627, and INT9814115.

commutation errors; see [2, 3, 9] for analysis of two kinds of commutation errors. The commutation errors are simply neglected in applications. Consider, e.g., the commutation error studied in [9]; its analysis shows that there are cases where it does not vanish asymptotically. A second serious problem of the classical LES in bounded domains is the definition of appropriate boundary conditions for the large scales. This problem is unresolved. In applications, often physically motivated wall laws are used. A possible remedy for this dilemma is the definition of the large scales in a different way, namely, by projection into appropriate spaces. This idea is the basis of variational multiscale methods (VMS); see [12]. VMS is part of a circle of ideas including the dynamic multilevel method by Dubois, Jauberteau, and Temam [8] and the additive turbulent decomposition; see Hylin and McDonough [15]. These approaches are related in spirit and philosophy but each has its own unique features.

Following Collis [6], the flow can be decomposed into three scales:

- (resolved) large scales,
- (resolved) small scales, and
- unresolved scales.

A VMS starts by writing the Navier–Stokes equations (1.1) as a coupled system of three equations for the three types of scales. Then, the equation for the unresolved scales is neglected and the equation for the resolved small scales will be modeled with a turbulence model; see section 3. In this way, the turbulence model acts directly only on the resolved small scales and it acts solely indirectly on the large scales by the coupling of the two remaining equations. One crucial point of a VMS is the definition of appropriate spaces which define the large scales and the resolved small scales. In [12], it is proposed to use a standard finite element space for the large scales and mesh cell bubbles for the resolved small scales. This resembles the idea of the residual free bubble approach for discretizing scalar convection-diffusion equations; e.g., see Brezzi et al. [4]. The advantage of this approach is that the equations for the resolved small scales can be solved mesh cell by mesh cell. However, using this approach in a VMS imposes the assumption that the resolved small scales exist only in the interior of mesh cells and they do not cross mesh cell faces. If the mesh is stationary, then the resolved scales are also stationary in some sense. They can change only within the mesh cells. It seems to be unlikely that this correctly reflects the behavior of the resolved small scales. An important feature of the VMS presented in this paper is that it does not have such a restriction. It allows the resolved small scales to move across faces of mesh cells.

In the VMS considered in this paper, a variationally consistent eddy viscosity turbulence model is introduced acting only on the discrete resolved small scales (fluctuations). This technique is inspired by Guermond [11] and Layton [25]. It can be also thought of as an extension of the spectral vanishing viscosity idea of Maday and Tadmor [26]. The VMS studied in the present paper is an extension of an approach for scalar convection-diffusion equations which can be found in [24]. It will be introduced in section 2. In contrast to the proposal in [12], it starts with a pair of finite element spaces which represents all resolved scales. There is one term where the turbulence model acts on all resolved scales. Then, a large scale space is chosen and in a second term, the action of the turbulence model on the large scales is subtracted again. The connection of this VMS to the VMS proposed in [12] is given in section 3. Section 4 derives conditions on the large scale space under which the VMS can be implemented easily and efficiently into an existing finite element code for Navier–Stokes equations. Finally, section 5 presents numerical studies with the VMS.

2. The VMS method. Throughout this paper, standard notations for Lebesgue and Sobolev spaces are used; e.g., see Adams [1]. The inner product in $(L^2(\Omega))^d$, $d \in \mathbb{N}$, is denoted by (\cdot, \cdot) .

Let $V = (H_0^1(\Omega))^d$ equipped with the norm $\|\mathbf{v}\|_V = \|\nabla \mathbf{v}\|_{L^2}$ and $Q = L_0^2(\Omega)$. A variational formulation of (1.1) reads as follows. Find $\mathbf{u} : [0, T] \rightarrow V$, $p : (0, T] \rightarrow Q$ satisfying

$$(2.1) \quad \begin{aligned} (\mathbf{u}_t, \mathbf{v}) + (2\nu \mathbb{D}(\mathbf{u}), \mathbb{D}(\mathbf{v})) + b(\mathbf{u}, \mathbf{u}, \mathbf{v}) - (p, \nabla \cdot \mathbf{v}) &= (\mathbf{f}, \mathbf{v}) \quad \forall \mathbf{v} \in V, \\ (q, \nabla \cdot \mathbf{u}) &= 0 \quad \forall q \in Q, \end{aligned}$$

and $\mathbf{u}(0, \mathbf{x}) = \mathbf{u}_0(\mathbf{x}) \in V$. Here, $\mathbb{D}(\mathbf{v}) = (\nabla \mathbf{v} + \nabla \mathbf{v}^T)/2$ is the velocity deformation tensor and $b(\mathbf{u}, \mathbf{v}, \mathbf{w}) = ((\mathbf{u} \cdot \nabla) \mathbf{v}, \mathbf{w})$. For the continuous problem, (2.1) is equivalent to a variational formulation where the viscous term has the form $(\nu \nabla \mathbf{u}, \nabla \mathbf{v})$.

As mentioned in the introduction, a Galerkin finite element discretization of (2.1) is unstable in the case of small viscosity (or high Reynolds number). A stabilization becomes necessary, which can be done, e.g., by introducing a turbulence model in (2.1). We consider the extension of an approach which was proposed in [24] for scalar convection-diffusion equations.

To keep the presentation concise, we will present the approach immediately for the semidiscrete problem. Let $V^h \subset V$ and $Q^h \subset Q$ be conforming finite element spaces which fulfill the inf-sup condition, i.e., there is a positive constant C independent of the mesh size parameter h such that

$$(2.2) \quad \inf_{q^h \in Q^h} \sup_{\mathbf{v}^h \in V^h} \frac{(\nabla \cdot \mathbf{v}^h, q^h)}{\|\nabla \mathbf{v}^h\|_{L^2} \|q^h\|_{L^2}} \geq C.$$

In addition, let $L^H \subset L = \{\mathbb{L} \in (L^2(\Omega))^{d \times d}, \mathbb{L} = \mathbb{L}^T\}$ and $\nu_T = \nu_T(t, \mathbf{x}, \mathbf{u}^h, p^h) \geq 0$. The semidiscrete problem (continuous in time) which we consider reads as follows. Find $\mathbf{u}^h : [0, T] \rightarrow V^h$, $p^h : (0, T] \rightarrow Q^h$ and $\mathbb{G}^H : [0, T] \rightarrow L^H$ satisfying

$$(2.3) \quad \begin{aligned} (\mathbf{u}_t^h, \mathbf{v}^h) + ((2\nu + \nu_T) \mathbb{D}(\mathbf{u}^h), \mathbb{D}(\mathbf{v}^h)) + b(\mathbf{u}^h, \mathbf{u}^h, \mathbf{v}^h) \\ - (p^h, \nabla \cdot \mathbf{v}^h) - (\nu_T \mathbb{G}^H, \mathbb{D}(\mathbf{v}^h)) &= (\mathbf{f}, \mathbf{v}^h) \quad \forall \mathbf{v}^h \in V^h, \\ (q^h, \nabla \cdot \mathbf{u}^h) &= 0 \quad \forall q^h \in Q^h, \\ (\mathbb{G}^H - \mathbb{D}(\mathbf{u}^h), \mathbb{L}^H) &= 0 \quad \forall \mathbb{L}^H \in L^H, \end{aligned}$$

and $\mathbf{u}^h(0, \mathbf{x}) = \mathbf{u}_0^h \in V^h$ is a discretely divergence-free approximation to \mathbf{u}_0 . Let $P_{L^H} : L \rightarrow L^H$, $\mathbb{D}(\mathbf{v}) \rightarrow P_{L^H} \mathbb{D}(\mathbf{v})$ with

$$(2.4) \quad (P_{L^H} \mathbb{D}(\mathbf{v}) - \mathbb{D}(\mathbf{v}), \mathbb{L}^H) = 0 \quad \forall \mathbb{L}^H \in L^H$$

denote the L^2 -projection from L onto L^H . Then $\mathbb{G}^H = P_{L^H} \mathbb{D}(\mathbf{u}^h)$ in (2.3).

The model within system (2.3) is determined by the choices of L^H and ν_T . The space L^H can be thought of as representing the large scales of the flow. Then, the application of ν_T in (2.3) can be interpreted as follows. In the viscous term (the second term in the first equation), the model (stabilization) is added to all scales, whereas in the last term of the left-hand side of the first equation, it is subtracted again for the large scales. Thus, the model, which is the only stabilization in the scheme, acts only on the small scales. This is exactly the main idea of the VMS of Hughes, Mazzei, and Jansen [12]. In this sense, (2.3) is a VMS; see the following section for a discussion of the connection of (2.3) to the VMS proposed in [12].

A finite element error analysis of the VMS (2.3) for the case that ν_T is a constant is presented in [21].

3. The connection to the VMS proposed in [12]. We consider the three-level partitioning of the flow given in the introduction. This partitioning will now be described by appropriate chosen function spaces. Clearly, the continuous pair of spaces (V, Q) contains all scales. The finite element spaces (V^h, Q^h) contain the large and the resolved small scales. Let $V^H \in (H^1(\Omega))^d$ be a discrete space such that $L^H = \mathbb{D}(V^H)$. The space V^H should be coarser than V^h in the sense that the piecewise polynomial degree of V^H is less than the piecewise polynomial degree of V^h . The functions of V^H may be defined on the same grid as the functions of V^h or on a coarser grid. But in the definition of V^H no boundary conditions, like no-slip conditions, are incorporated. Thus, in general $V^H \not\subset V^h$. The large eddies of a turbulent flow generally do not fulfill no-slip boundary conditions, e.g., the large eddies of a hurricane move along the surface of the earth. Thus, it make sense not to incorporate such boundary conditions into the definition of V^H . The pair of spaces for the large scales is given by (V^H, Q^H) , where Q^H is chosen such that an inf-sup condition of type (2.2) is fulfilled for (V^H, Q^H) . The large scales $P_H \mathbf{u}$ of the velocity are defined by an elliptic projection into V^H and the large scales $P_H p$ of the pressure by the L^2 -projection into Q^H ; $P_H : (V, Q) \rightarrow (V^H, Q^H)$,

$$(3.1) \quad \begin{aligned} (\mathbb{D}(\mathbf{u} - P_H \mathbf{u}), \mathbb{D}(\mathbf{v}^H)) &= 0 \quad \forall \mathbf{v}^H \in V^H, \\ (\mathbf{u} - P_H \mathbf{u}, 1) &= 0, \\ (p - P_H p, q^H) &= 0 \quad \forall q^H \in Q^H. \end{aligned}$$

The following lemma shows that this choice is consistent in the following sense: the deformation tensor of the large scales defined in (3.1) is equal to the large scales of the deformation tensor defined in (2.4). That means that differentiation and the definition of the large scales (by projection) commute. We like to recall that this property in general is not valid in the classical LES.

LEMMA 3.1. *Let $\mathbf{v} \in V$ and $L^H = \mathbb{D}(V^H)$. Then*

$$(3.2) \quad P_{L^H} \mathbb{D}(\mathbf{v}) = \mathbb{D}(P_H \mathbf{v}) \quad \forall \mathbf{v} \in V.$$

Proof. From $L^H = \mathbb{D}(V^H)$ and $P_{L^H} \mathbb{D}(\mathbf{v}) \in L^H$ follow that there is a $\mathbf{w}^H \in V^H$ such that $P_{L^H} \mathbb{D}(\mathbf{v}) = \mathbb{D}(\mathbf{w}^H)$. Using (2.4) gives

$$(3.3) \quad (\mathbb{D}(\mathbf{v} - \mathbf{w}^H), \mathbb{L}^H) = 0 \quad \forall \mathbb{L}^H \in L^H.$$

On the other hand, since $L^H = \mathbb{D}(V^H)$, (3.1) is equivalent to

$$(3.4) \quad (\mathbb{D}(\mathbf{v} - P_H \mathbf{v}), \mathbb{L}^H) = 0 \quad \forall \mathbb{L}^H \in L^H.$$

The statement of the lemma follows now directly from (3.3) and (3.4) since the elliptic projection is unique. \square

Let ν_T be a constant. A straightforward calculation shows that

$$\begin{aligned} &(\nu_T \mathbb{D}(\mathbf{u}^h), \mathbb{D}(\mathbf{v}^h)) - (\nu_T P_{L^H} \mathbb{D}(\mathbf{u}^h), \mathbb{D}(\mathbf{v}^h)) \\ &= (\nu_T (I - P_{L^H}) \mathbb{D}(\mathbf{u}^h), (I - P_{L^H}) \mathbb{D}(\mathbf{v}^h)). \end{aligned}$$

Thus, system (2.3) can be reformulated as follows. Find $\mathbf{u}^h : [0, T] \rightarrow V^h$, $p^h : (0, T] \rightarrow Q^h$ satisfying

$$(3.5) \quad \begin{aligned} &(\mathbf{u}_t^h, \mathbf{v}^h) + (2\nu \mathbb{D}(\mathbf{u}^h), \mathbb{D}(\mathbf{v}^h)) + b(\mathbf{u}^h, \mathbf{u}^h, \mathbf{v}^h) \\ &- (p^h, \nabla \cdot \mathbf{v}^h) + (\nu_T (I - P_{L^H}) \mathbb{D}(\mathbf{u}^h), (I - P_{L^H}) \mathbb{D}(\mathbf{v}^h)) = (\mathbf{f}, \mathbf{v}^h) \quad \forall \mathbf{v}^h \in V^h, \\ &(q^h, \nabla \cdot \mathbf{u}^h) = 0 \quad \forall q^h \in Q^h. \end{aligned}$$

Decompose now $V^h = V^H + \tilde{V}^h$, $Q^h = Q^H + \tilde{Q}^h$ with $\tilde{V}^h = (I - P_H)V^h$. It follows with (3.2) that

$$(3.6) \quad (I - P_{L^H})\mathbb{D}(\mathbf{v}^h) = \mathbb{D}(\mathbf{v}^h - P_H\mathbf{v}^h) = \mathbb{D}((I - P_H)\mathbf{v}^h).$$

If $\mathbf{v}^H \in V^H$, we have $\mathbb{D}(\mathbf{v}^H) = \mathbb{D}(P_H\mathbf{v}^H)$. Thus, a straightforward calculation shows that the momentum equation in (3.5) becomes for all test functions $\mathbf{v}^H \in V^H$

$$(3.7) \quad \begin{aligned} & (\mathbf{u}_t^H, \mathbf{v}^H) + (2\nu\mathbb{D}(\mathbf{u}^H), \mathbb{D}(\mathbf{v}^H)) + b(\mathbf{u}^H, \mathbf{u}^H, \mathbf{v}^H) - (p^H, \nabla \cdot \mathbf{v}^H) + (\tilde{\mathbf{u}}_t^h, \mathbf{v}^H) \\ & \quad + (2\nu\mathbb{D}(\tilde{\mathbf{u}}^h), \mathbb{D}(\mathbf{v}^H)) + b(\mathbf{u}^H, \tilde{\mathbf{u}}^h, \mathbf{v}^H) + b(\tilde{\mathbf{u}}^h, \mathbf{u}^H, \mathbf{v}^H) - (p^h, \nabla \cdot \mathbf{v}^H) \\ & = (\mathbf{f}, \mathbf{v}^H) - b(\tilde{\mathbf{u}}^h, \tilde{\mathbf{u}}^h, \mathbf{v}^H). \end{aligned}$$

The definition of \tilde{V}^h , (3.6), and a direct calculation show that

$$(3.8) \quad \begin{aligned} & (\tilde{\mathbf{u}}_t^h, \tilde{\mathbf{v}}^h) + (2\nu\mathbb{D}(\tilde{\mathbf{u}}^h), \mathbb{D}(\tilde{\mathbf{v}}^h)) + b(\tilde{\mathbf{u}}^h, \tilde{\mathbf{u}}^h, \tilde{\mathbf{v}}^h) - (\tilde{p}^h, \nabla \cdot \tilde{\mathbf{v}}^h) + (\nu_T\mathbb{D}(\tilde{\mathbf{u}}^h), \mathbb{D}(\tilde{\mathbf{v}}^h)) \\ & \quad = (\mathbf{f}, \tilde{\mathbf{v}}^h) - (\mathbf{u}_t^H, \tilde{\mathbf{v}}^h) - (2\nu\mathbb{D}(\mathbf{u}^H), \mathbb{D}(\tilde{\mathbf{v}}^h)) - b(\tilde{\mathbf{u}}^h, \mathbf{u}^H, \tilde{\mathbf{v}}^h) - b(\mathbf{u}^H, \tilde{\mathbf{u}}^h, \tilde{\mathbf{v}}^h) \\ & \quad + (p^H, \nabla \cdot \tilde{\mathbf{v}}^h) \end{aligned}$$

for all $\tilde{\mathbf{v}}^h \in \tilde{V}^h$. The coupled system (3.7), (3.8) possesses exactly the form of the VMS proposed in [12]. The unresolved scales are modeled only in the small scale equation (3.8). In [12, 13, 14], eddy viscosity models of Smagorinsky type have been used. There is no model in (3.7) for the large scales. The model of the unresolved scales influences the large scales only indirectly by the coupling of (3.7) and (3.8).

4. Aspects of the implementation. This section describes some aspects of implementing (2.3) into a finite element code. One has two options for defining the large scale space L^H . The first option is to define L^H on a coarser grid than (V^h, Q^h) . Since, we will use higher order finite element spaces for (V^h, Q^h) , there is as second option to define L^H on the same grid as (V^h, Q^h) using lower order polynomials. We will use the second way. It will be shown that in this case an efficient implementation with only small modifications of an existing code for solving the Navier–Stokes equations is possible if L^H is a discontinuous finite element space with a L^2 -orthogonal basis. We will describe the implementation for three dimensions; the modifications in two dimensions are obvious.

Let the velocity vector \mathbf{u}^h and the symmetric tensor \mathbb{G}^H be given by

$$\mathbf{u}^h = \begin{pmatrix} u_1^h \\ u_2^h \\ u_3^h \end{pmatrix}, \quad \mathbb{G}^H = \begin{pmatrix} g_{11}^H & g_{12}^H & g_{13}^H \\ g_{12}^H & g_{22}^H & g_{23}^H \\ g_{13}^H & g_{23}^H & g_{33}^H \end{pmatrix}$$

and let the spaces V^h and L^H be equipped with the bases

$$(4.1) \quad \begin{aligned} V^h &= \text{span} \left\{ \left(\begin{pmatrix} v_i^h \\ 0 \\ 0 \end{pmatrix}, \begin{pmatrix} 0 \\ v_i^h \\ 0 \end{pmatrix}, \begin{pmatrix} 0 \\ 0 \\ v_i^h \end{pmatrix} : i = 1, \dots, n_V \right\}, \\ L^H &= \text{span} \left\{ \left(\begin{pmatrix} l_j^H & 0 & 0 \\ 0 & 0 & 0 \\ 0 & 0 & 0 \end{pmatrix}, \frac{1}{2} \begin{pmatrix} 0 & l_j^H & 0 \\ l_j^H & 0 & 0 \\ 0 & 0 & 0 \end{pmatrix}, \frac{1}{2} \begin{pmatrix} 0 & 0 & l_j^H \\ 0 & 0 & 0 \\ l_j^H & 0 & 0 \end{pmatrix}, \right. \\ & \quad \left. \begin{pmatrix} 0 & 0 & 0 \\ 0 & l_j^H & 0 \\ 0 & 0 & 0 \end{pmatrix}, \frac{1}{2} \begin{pmatrix} 0 & 0 & 0 \\ 0 & 0 & l_j^H \\ 0 & l_j^H & 0 \end{pmatrix}, \begin{pmatrix} 0 & 0 & 0 \\ 0 & 0 & 0 \\ 0 & 0 & l_j^H \end{pmatrix} : j = 1, \dots, n_L \right\}. \end{aligned}$$

After an implicit discretization of (2.3) in time and an appropriate linearization of the convective term in the current time step, one obtains a linear saddle point problem of the following form:

$$(4.2) \quad \begin{pmatrix} A_{11} & A_{12} & A_{13} & B_1^T & \tilde{G}_{11} & \tilde{G}_{12} & \tilde{G}_{13} & \tilde{G}_{14} & \tilde{G}_{15} & \tilde{G}_{16} \\ A_{21} & A_{22} & A_{23} & B_2^T & \tilde{G}_{21} & \tilde{G}_{22} & \tilde{G}_{23} & \tilde{G}_{24} & \tilde{G}_{25} & \tilde{G}_{26} \\ A_{31} & A_{32} & A_{33} & B_3^T & \tilde{G}_{31} & \tilde{G}_{32} & \tilde{G}_{33} & \tilde{G}_{34} & \tilde{G}_{35} & \tilde{G}_{36} \\ B_1 & B_2 & B_3 & 0 & 0 & 0 & 0 & 0 & 0 & 0 \\ G_{11} & G_{12} & G_{13} & 0 & M & 0 & 0 & 0 & 0 & 0 \\ G_{21} & G_{22} & G_{23} & 0 & 0 & \frac{M}{2} & 0 & 0 & 0 & 0 \\ G_{31} & G_{32} & G_{33} & 0 & 0 & 0 & \frac{M}{2} & 0 & 0 & 0 \\ G_{41} & G_{42} & G_{43} & 0 & 0 & 0 & 0 & M & 0 & 0 \\ G_{51} & G_{52} & G_{53} & 0 & 0 & 0 & 0 & 0 & \frac{M}{2} & 0 \\ G_{61} & G_{62} & G_{63} & 0 & 0 & 0 & 0 & 0 & 0 & M \end{pmatrix} \begin{pmatrix} u_1^h \\ u_2^h \\ u_3^h \\ p^h \\ g_{11}^H \\ g_{12}^H \\ g_{13}^H \\ g_{22}^H \\ g_{23}^H \\ g_{33}^H \end{pmatrix} = \begin{pmatrix} f_1^h \\ f_2^h \\ f_3^h \\ 0 \\ 0 \\ 0 \\ 0 \\ 0 \\ 0 \\ 0 \end{pmatrix}.$$

The matrices A_{11}, \dots, A_{33} and B_1, B_2, B_3 have to be assembled if (2.3) is discretized without the terms involving G^H , i.e., if all scales are stabilized. The matrix M in (4.2) is the mass matrix of L^H : $(M)_{ij} = (l_j^H, l_i^H)$. The general entries of the matrices G_{11}, \dots, G_{63} and $\tilde{G}_{11}, \dots, \tilde{G}_{36}$ can be computed easily by using the bases of V^h and L^H . Straightforward calculations give

$$(4.3) \quad \begin{aligned} (G_{11})_{ij} &= \left(\begin{pmatrix} (v_j^h)_x & (v_j^h)_y/2 & (v_j^h)_z/2 \\ (v_j^h)_y/2 & 0 & 0 \\ (v_j^h)_z/2 & 0 & 0 \end{pmatrix}, \begin{pmatrix} l_i^H & 0 & 0 \\ 0 & 0 & 0 \\ 0 & 0 & 0 \end{pmatrix} \right) \\ &= ((v_j^h)_x, l_i^H) & G_{22} &= G_{33} = \frac{1}{2}G_{11}, \\ (G_{42})_{ij} &= ((v_j^h)_y, l_i^H) & G_{21} &= G_{53} = \frac{1}{2}G_{42}, \\ (G_{63})_{ij} &= ((v_j^h)_z, l_i^H) & G_{31} &= G_{52} = \frac{1}{2}G_{63}, \\ (\tilde{G}_{11})_{ij} &= (\nu_T l_j^H, (v_i^h)_x) & \tilde{G}_{22} &= \tilde{G}_{33} = \frac{1}{2}\tilde{G}_{11}, \\ (\tilde{G}_{24})_{ij} &= (\nu_T l_j^H, (v_i^h)_y) & \tilde{G}_{12} &= \tilde{G}_{35} = \frac{1}{2}\tilde{G}_{24}, \\ (\tilde{G}_{36})_{ij} &= (\nu_T l_j^H, (v_i^h)_z) & \tilde{G}_{13} &= \tilde{G}_{25} = \frac{1}{2}\tilde{G}_{36}. \end{aligned}$$

All other blocks $G_{\alpha\beta}$ and $\tilde{G}_{\alpha\beta}$ vanish. Thus, one has to assemble only the entries of the blocks $G_{11}, G_{42}, G_{63}, \tilde{G}_{11}, \tilde{G}_{24}, \tilde{G}_{36}$. The assembling of the last three blocks is not necessary if ν_T is constant. The matrices G_{11}, G_{42}, G_{63} , and M have to be assembled only once since they are not time dependent. The matrices $\tilde{G}_{11}, \tilde{G}_{24}, \tilde{G}_{36}$ are time dependent iff ν_T is time dependent, e.g., if ν_T depends on the solution as in the numerical studies presented in section 5.

Now, (4.2) can be solved for $g_{11}^H, \dots, g_{33}^H$. This leads to a saddle point problem for (\mathbf{u}^h, p^h) of the form

$$(4.4) \quad \begin{pmatrix} \tilde{A}_{11} & \tilde{A}_{12} & \tilde{A}_{13} & B_1^T \\ \tilde{A}_{21} & \tilde{A}_{22} & \tilde{A}_{23} & B_2^T \\ \tilde{A}_{31} & \tilde{A}_{32} & \tilde{A}_{33} & B_3^T \\ B_1 & B_2 & B_3 & 0 \end{pmatrix} \begin{pmatrix} u_1^h \\ u_2^h \\ u_3^h \\ p^h \end{pmatrix} = \begin{pmatrix} f_1^h \\ f_2^h \\ f_3^h \\ 0 \end{pmatrix}$$

with

$$\begin{aligned} \tilde{A}_{11} &= A_{11} - \tilde{G}_{11}M^{-1}G_{11} - \frac{1}{2}\tilde{G}_{24}M^{-1}G_{42} - \frac{1}{2}\tilde{G}_{36}M^{-1}G_{63}, \\ \tilde{A}_{12} &= A_{12} - \frac{1}{2}\tilde{G}_{24}M^{-1}G_{11}, \\ \tilde{A}_{13} &= A_{13} - \frac{1}{2}\tilde{G}_{36}M^{-1}G_{11}, \\ &\vdots \\ \tilde{A}_{33} &= A_{33} - \tilde{G}_{36}M^{-1}G_{63} - \frac{1}{2}\tilde{G}_{11}M^{-1}G_{11} - \frac{1}{2}\tilde{G}_{24}M^{-1}G_{42}. \end{aligned}$$

Note that a different scaling of the basis functions of L^H leads to the same formulas.

Let \mathcal{T}^h be triangulation of Ω with mesh cells K and let $(\cdot, \cdot)_K$ denote the inner product in $L^2(K)$. The (i, j) th entry of $\tilde{G}_{11}M^{-1}G_{11}$ has the form

$$\begin{aligned} (\tilde{G}_{11}M^{-1}G_{11})_{ij} &= \sum_{m,n=1}^{n_L} (\tilde{G}_{11})_{im}(M^{-1})_{mn}(G_{11})_{nj} \\ (4.5) \quad &= \sum_{m,n=1}^{n_L} (\nu_T l_m^H, (v_i^h)_x)(M^{-1})_{mn}((v_j^h)_x, l_n^H) \\ &= \sum_{m,n=1}^{n_L} \left(\sum_{K \in \mathcal{T}^h} (\nu_T l_m^H, (v_i^h)_x)_K \right) (M^{-1})_{mn} \left(\sum_{K \in \mathcal{T}^h} ((v_j^h)_x, l_n^H)_K \right). \end{aligned}$$

This formula reveals that for an easy and efficient implementation of the method into an existing code, two requirements have to be fulfilled.

First, an efficient computation of (4.5) is possible if M is a diagonal matrix. This holds iff the basis functions of L^H are L^2 -orthogonal. One obtains in this case

$$(4.6) \quad (\tilde{G}_{11}M^{-1}G_{11})_{ij} = \sum_{m=1}^{n_L} \frac{\sum_{K \in \mathcal{T}^h} (\nu_T l_m^H, (v_i^h)_x)_K \sum_{K \in \mathcal{T}^h} ((v_j^h)_x, l_m^H)_K}{\sum_{K \in \mathcal{T}^h} (l_m^H, l_m^H)_K}.$$

For a nonorthogonal basis, one can use the approximation $(\text{diag}(M))^{-1}$ instead of M^{-1} or some other diagonal matrix which is derived from M , e.g., by adding all matrix entries in a row to the diagonal.

Second, the sparsity pattern of $\tilde{A}_{\alpha\beta}$ must not be larger than the sparsity pattern of $A_{\alpha\beta}$. Then, the entries coming from terms like (4.6) can be simply added to $A_{\alpha\beta}$. An entry $(A_{\alpha\beta})_{ij}$ generally does not vanish if the intersection of the support of v_i^h and the support of v_j^h is at least one mesh cell K . If the support of l_m^H is only one mesh cell, then the numerator in (4.6) may be not equal to zero only if this mesh cell belongs also to the support of v_i^h and to the support of v_j^h . In this case, the sparsity pattern of $\tilde{G}_{11}M^{-1}G_{11}$ (and hence of \tilde{A}_{11}) will be the same as of A_{11} . The requirement on the support of l_m^H can be fulfilled if L^H is a discontinuous finite element space.

If the support of l_m^H consists of more than one mesh cell, the sparsity pattern of $\tilde{G}_{11}M^{-1}G_{11}$ will in general be larger than that of A_{11} . In this case, one can use an approximation of $\tilde{G}_{11}M^{-1}G_{11}$ where all entries which do not belong to the sparsity pattern of A_{11} are dropped (similar to the standard approach for an ILU decomposition).

Examples of spaces L^H fulfilling both requirements are given in section 5.

Since (4.4) has the same form as the Galerkin discretization of the Navier–Stokes equations, existing solvers of a code for this discretizations can be used as well for (4.4).

The implementation of this approach in the code MoonMD [23], which was used in the computations presented in section 5, is as follows. The matrices M , G_{11} , G_{42} , and G_{63} are assembled once at the initial time. The matrices $\tilde{A}_{\alpha\beta}$, \tilde{G}_{11} , \tilde{G}_{24} , and \tilde{G}_{36} have to be assembled in each step of the iterative scheme to solve the nonlinear equation in each discrete time. We start by assembling $A_{\alpha\beta}$, \tilde{G}_{11} , \tilde{G}_{24} , and \tilde{G}_{36} . Then all necessary matrix products $\tilde{G}_{ij}M^{-1}G_{kl}$ are computed and subtracted from $A_{\alpha\beta}$ to obtain $\tilde{A}_{\alpha\beta}$. The computational overhead of the second step is studied in section 5.3.

In summary, using for L^H a discontinuous finite element space with an L^2 -orthogonal basis leads to a system of form (4.4) where the matrices \tilde{A}_{ij} have the same sparsity pattern as A_{ij} . Solvers for the Navier–Stokes equations which are already implemented can be applied immediately to (4.4). The only extension of an existing code for the Navier–Stokes equations consists of assembling the matrices \tilde{A}_{ij} instead of A_{ij} .

5. Numerical studies. Given a turbulent viscosity ν_T , the amount of modeling in the VMS studied in this paper is determined by the choice of the space L^H . If $L^H = \{\mathbb{O}\}$, the model acts on all resolved scales. The larger $L^H \subseteq \mathbb{D}(V^h)$ is chosen, the less scales are influenced by the model and the closer the computed solution should be to the solution of the Navier–Stokes equations discretized by the Galerkin finite element method. The numerical studies in sections 5.1 and 5.2 will support this expectation. Finally, section 5.3 studies a turbulent flow around a cylinder.

In the numerical studies, the Smagorinsky model [31]

$$(5.1) \quad \nu_T = c_S \delta^2 \|\mathbb{D}(\mathbf{u}^h)\|_F$$

is used for the turbulent viscosity. Here, c_S is a constant, δ is the filter width of LES, which is related to the mesh width, and $\|\cdot\|_F$ denotes the Frobenius norm of a tensor. The Smagorinsky model is a simple and popular LES model; e.g., see [30] for its advantages and drawbacks. It was used in the computations with the VMS presented in [13, 14].

We will present computations on hexahedral grids with the pair of mapped finite element spaces (Q_2, P_1^{disc}) . Here, Q_2 is the space of continuous piecewise triquadratic functions and P_1^{disc} is the space of discontinuous piecewise linears. This pair of finite element spaces is considered currently among the best performers in the numerical simulation of incompressible flows; see [10, 22, 16].

The basis functions of Q_2 on the reference cube are $\{\xi^i \eta^j \zeta^l, i, j, l = 0, 1, 2\}$. Thus, the deformation tensor of functions from Q_2 contains all polynomials up to degree 1 and even polynomials of higher order. This gives a guideline for choosing $L^H \subseteq \mathbb{D}(V^h)$. In our computations, we use for L^H discontinuous finite element spaces P_k^{disc} , $k \in \{0, 1\}$, containing piecewise constants or linears, respectively. It is easy to equip these spaces with L^2 -orthogonal bases of piecewise Legendre polynomials.

As temporal discretization, the fractional-step θ -scheme [5] is applied in sections 5.1 and 5.2 and the Crank–Nicolson scheme in section 5.3. These fully implicit second order schemes are among the most popular time stepping schemes in incompressible flow computations [32].

The nonlinear problem in each discrete time was linearized by a fixed point iteration. In each step of the fixed point iteration, a linear saddle point problem, a

so-called Oseen problem, has to be solved. We used as solver a preconditioned flexible GMRES method [29] with a multilevel preconditioner. This solver is described in detail in [16, 18]. The computations were performed with the code MooNMD [18, 23].

5.1. The flow through a three-dimensional channel. We consider the flow through the channel $\Omega = (0, 10) \times (0, 1) \times (0, 1)$. At the inflow boundary $x = 0$, the steady state inflow

$$\mathbf{u}(t, 0, y, z) = \begin{pmatrix} 4y(1-y) \\ 0 \\ 0 \end{pmatrix} =: \mathbf{U},$$

at the boundaries $y = 0$ and $y = 1$ no-slip conditions $\mathbf{u} = \mathbf{0}$, and at the boundaries $z = 0$ and $z = 1$ free slip conditions are prescribed. The implementation of the free slip conditions into MooNMD is described in [17]. The flow leaves the channel at $x = 10$ by outflow boundary conditions. The initial velocity is given by $\mathbf{u}(0, x, y, z) = \mathbf{U}$ and the right-hand side is chosen to be $\mathbf{f} = \mathbf{0}$. The solution of the Navier–Stokes equations (1.1) of this channel flow is

$$(5.2) \quad \mathbf{u}(t, x, y, z) = \mathbf{U}, \quad p(t, x, y, z) = -8\nu(x - 10).$$

We present results of computations with the viscosity $\nu^{-1} = 10^5$ and the final time $T = 20$. The Reynolds number of the flow, based on the average inflow U and the height of the channel $L = 1$, is

$$Re = \frac{UL}{\nu} = \frac{2}{3}10^5 \approx 66667.$$

The initial grid (level 0) consists of 80 cubes of size $h = 0.5$. The computations were carried out on levels 1 ($h = 0.25$) and 2 ($h = 0.125$). On level 1, there are 19,683 degrees of freedom (d.o.f.) of the velocity and 2,560 d.o.f. of the pressure. The number of d.o.f. on level 2 is 139,587 for the velocity and 20,480 for the pressure. The filter width in the Smagorinsky model (5.1) was chosen to be $\delta = 2h$. For the constant, $c_S = 0.01$ was used. These are typical values. The fractional-step θ -scheme was applied with equidistant time steps of length 0.01.

The quantities of interest which we consider are the errors $\mathbf{U} - \mathbf{u}^h$ in different norms (see Table 5.1) and the total kinetic energy of the flow given by

$$E_{\text{kin}}(\mathbf{u}) = \frac{1}{2} \int_{\Omega} \mathbf{u}^T \mathbf{u} \, d\mathbf{x} \quad \text{for } t \in [0, T].$$

The total kinetic energy of (5.2) is $2.6\bar{6}\bar{6}$ for each time t .

The solution (5.2) of the Navier–Stokes equations is contained in the ansatz space (V^h, Q^h) and it is steady state. Thus, the Galerkin finite element discretization computes in this example exactly this solution. However, slight perturbations of the initial or inflow condition lead to a blow-up of the Galerkin finite element method (FEM) solution.

The numerical results are presented in Table 5.1 and Figure 5.1. Modeling all scales by the Smagorinsky model often gives the largest errors to the solution of the Navier–Stokes equations and always gives the largest difference of the total kinetic energy. Choosing the small space $L^H = P_0^{\text{disc}}$ in the VMS often gives somewhat smaller errors. If one uses $L^H = P_1^{\text{disc}}$ in the VMS, one obtains solutions in this

TABLE 5.1
Three-dimensional channel flow, errors of the velocity in different norms.

Level	Error	Smagorinsky	VMS, $L^H = P_0^{\text{disc}}$	VMS, $L^H = P_1^{\text{disc}}$
1	$L^\infty(0, T; L^2)$	1.186e-1	7.606e-2	3.428e-5
1	$L^2(0, T; L^2)$	4.807e-1	3.260e-1	1.332e-4
1	$L^2(0, T; H^1)$	4.672	7.7016	3.738e-3
2	$L^\infty(0, T; L^2)$	6.064e-2	1.612e-2	5.609e-5
2	$L^2(0, T; L^2)$	2.285e-1	6.943e-2	2.029e-4
2	$L^2(0, T; H^1)$	2.167	3.657	1.020e-2

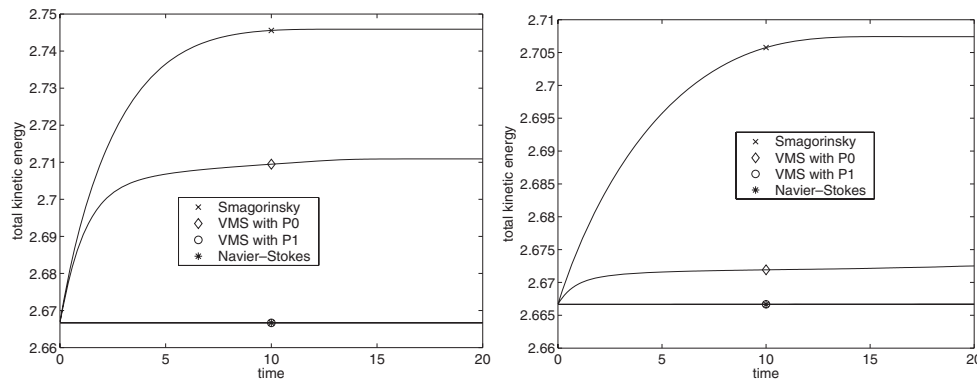


FIG. 5.1. *Three-dimensional channel flow, total kinetic energy. Left, level 1; right, level 2.*

channel flow example which are nearly identical with the solution of the Navier–Stokes equations. The refinement in space from level 1 to level 2 results in a decrease of the errors and in the difference of the total kinetic energy for the Smagorinsky model and the VMS with $L^H = P_0^{\text{disc}}$. For the VMS with $L^H = P_1^{\text{disc}}$, the errors seem to be dominated by the discretization error in time.

5.2. A three-dimensional mixing layer problem. The mixing layer problem is an often used test problem for turbulent flow simulations in three dimensions. Computations with this problem can be found, e.g., in Comte, Lesieur, and Lamballais [7], Rogers and Moser [28], Vreman, Guerts, and Kuerten [33], and [19].

The domain of computation is $\Omega = (-1, 1) \times (-2, 2) \times (0, 2)$. Free slip boundary conditions are applied at $y = -2$ and $y = 2$. On the other four boundaries, periodic boundary conditions are prescribed. The initial velocity is given by

$$(5.3) \quad \mathbf{u}_0 = \begin{pmatrix} U_\infty \tanh\left(\frac{2y}{\sigma_0}\right) \\ 0 \\ 0 \end{pmatrix} + c_{\text{noise}} U_\infty \begin{pmatrix} \frac{\partial \psi}{\partial y} + \frac{\partial \psi}{\partial z} \\ -\frac{\partial \psi}{\partial x} \\ -\frac{\partial \psi}{\partial x} \end{pmatrix}$$

with $\psi = \exp(-(2y/\sigma_0)^2)(\cos(\pi x) + \cos(2\pi z))$. We will present computations with $\nu^{-1} = 700$, $U_\infty = 1$, $c_{\text{noise}} = 0.01$, and the initial vorticity thickness $\sigma_0 = 1/14$. Defining the Reynolds number by $Re = \sigma_0 U_\infty \nu^{-1}$ gives a flow with $Re = 50$.

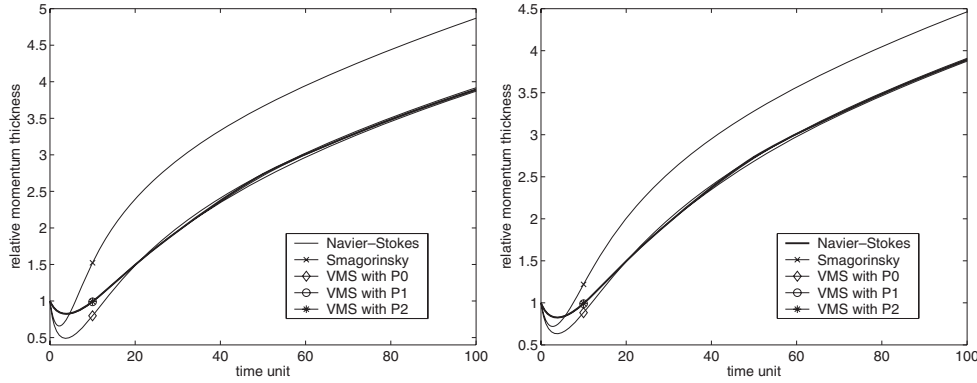


FIG. 5.2. Three-dimensional mixing layer problem, relative momentum thickness, $c_S = 0.01$ (left), $c_S = 0.005$ (right).

A time unit \bar{t} is defined by $\bar{t} = \sigma_0/U_\infty$. The fractional-step θ -scheme was applied with an equidistant time step of $\Delta t_n = 0.5\bar{t} = 1/28 \approx 0.035714$ and the final time was set to $T = 100\bar{t} \approx 7.1428$. The initial grid (level 0, $h = \sqrt{3}$) consists of 16 cubes of edge length one. This grid is refined uniformly. The computations are carried out on level 3, $h = \sqrt{3}/8$ (199,680 d.o.f. for the velocity, 32,768 d.o.f. for the pressure). In the Smagorinsky model (5.1), the filter width $\delta = h$ and the scaling parameters $c_S = 0.01$ and $c_S = 0.005$ were used.

The computational results are evaluated using the relative momentum thickness (Figures 5.2 and 5.4), the total kinetic energy (Figures 5.3 and 5.4), and plots of the z -component of the vorticity in the plane $z = 1$ (Figures 5.5 and 5.6), where the part $(-1, 1) \times (-1, 1)$ of the cut plane is presented. The vorticity of a vector field $\mathbf{u} = (u_1, u_2, u_3)^T$ is given by

$$\boldsymbol{\omega} = \nabla \times \mathbf{u} = \begin{pmatrix} (u_3)_y - (u_2)_z \\ (u_1)_z - (u_3)_y \\ (u_2)_x - (u_1)_y \end{pmatrix}.$$

Let $\Omega = (x_0, x_1) \times (-y_0, y_0) \times (z_0, z_1)$ with $y_0 > 0$. The momentum thickness $\mu(t)$ is a typical quantity which is considered in the three-dimensional mixing layer problem. It is given by

$$\mu(t) = \int_{-y_0}^{y_0} \left(\frac{1}{4} - \left(\frac{\langle u_1 \rangle(t, y)}{2U_\infty} \right)^2 \right) dy,$$

where

$$\langle u_1 \rangle(t, y) = \frac{\int_{x_0}^{x_1} \int_{z_0}^{z_1} u_1(t, x, y, z) dz dx}{\int_{x_0}^{x_1} \int_{z_0}^{z_1} dz dx}.$$

The momentum thickness of the discrete initial velocity is $\mu(0) = 2.108548e - 2$ and the relative momentum thickness is defined by $\mu(t)/\mu(0)$.

In this example, we used the VMS also with $L^H = P_2^{\text{disc}}$, although in this case $L^H \not\subseteq \mathbb{D}(V^h)$. A local basis, i.e., a basis in each mesh cell, of the scalar space P_2^{disc} is

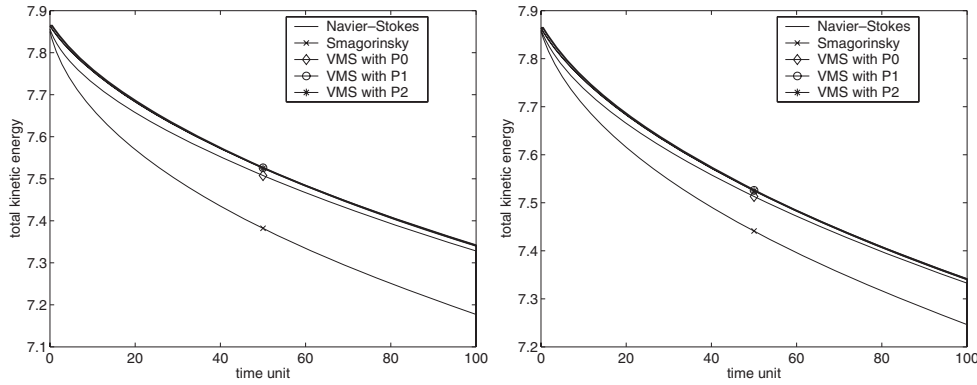


FIG. 5.3. Three-dimensional mixing layer problem, total kinetic energy, $c_S = 0.01$ (left), $c_S = 0.005$ (right).

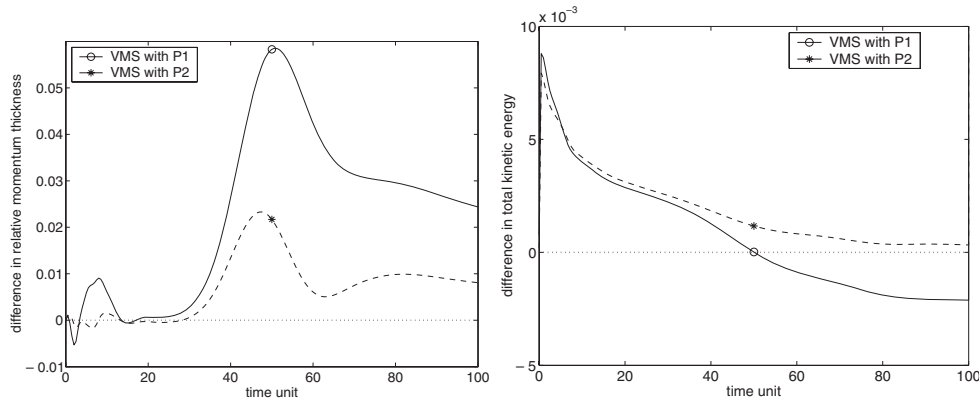


FIG. 5.4. Three-dimensional mixing layer problem, $c_S = 0.01$, differences of using $L^H = P_1^{\text{disc}}$ and $L^H = P_2^{\text{disc}}$ in the VMS to the Galerkin discretization of the Navier–Stokes equations, relative momentum thickness (left), total kinetic energy (right).

the set $\{\xi^i \eta^j \zeta^l, 0 \leq i + j + l \leq 2\}$. This set contains 10 functions. Accordingly, the local basis of the symmetric tensor space P_2^{disc} has the dimension 60; see (4.1). The restriction of $\mathbb{D}(V^h)$ to a mesh cell contains 57 of these basis functions. Not contained in $\mathbb{D}(V^h)$ are

$$\begin{pmatrix} \xi^2 & 0 & 0 \\ 0 & 0 & 0 \\ 0 & 0 & 0 \end{pmatrix}, \begin{pmatrix} 0 & 0 & 0 \\ 0 & \eta^2 & 0 \\ 0 & 0 & 0 \end{pmatrix}, \begin{pmatrix} 0 & 0 & 0 \\ 0 & 0 & 0 \\ 0 & 0 & \eta^2 \end{pmatrix}.$$

On the other hand, $\mathbb{D}(V^h)$ contains also functions which do not belong to $L^H = P_2^{\text{disc}}$.

The computational results agree completely with the expectations. The larger L^H is chosen, the closer become the results of the VMS to the results obtained with the Galerkin discretization of the Navier–Stokes equations. Using the Smagorinsky model, $L^H = \{\mathbb{O}\}$, one can observe for both values of c_S that it is too diffusive. The eddies in the flow are quickly smoothed out; see the second row in Figures 5.5 and 5.6. Although the relative momentum thickness and the total kinetic energy with

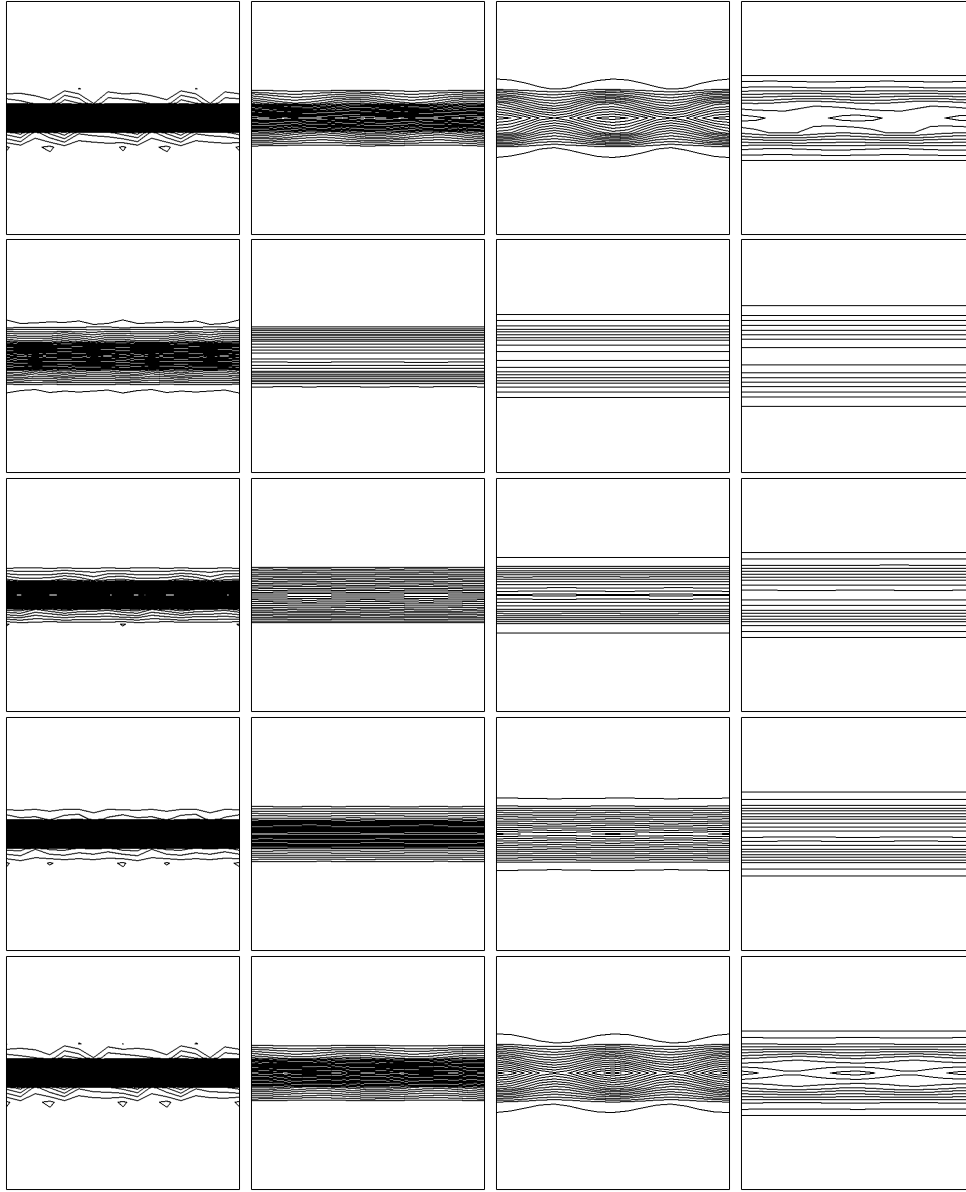


FIG. 5.5. Three-dimensional mixing layer problem, vorticity at time units 10, 30, 60, 100 (left to right), Galerkin FEM, Smagorinsky model with $c_S = 0.01$, VMS with $L^H = P_0^{\text{disc}}$, VMS with $L^H = P_1^{\text{disc}}$, VMS with $L^H = P_2^{\text{disc}}$ (top to bottom).

$L^H = P_0^{\text{disc}}$ are much closer to the curves obtained for the Navier–Stokes equations, there is only a small improvement visible in the vorticity plots; see the third row in Figures 5.5 and 5.6. The curves of the relative momentum thickness and the total kinetic energy are almost identical for $L^H = P_1^{\text{disc}}$ and $L^H = P_2^{\text{disc}}$. But the plots of the vorticity show the great improvement which is achieved with $L^H = P_2^{\text{disc}}$; compare the fourth and fifth rows in Figures 5.5 and 5.6. For $c_S = 0.01$, the solution is very similar to the solution for the Navier–Stokes equations, at least up to time unit 60.

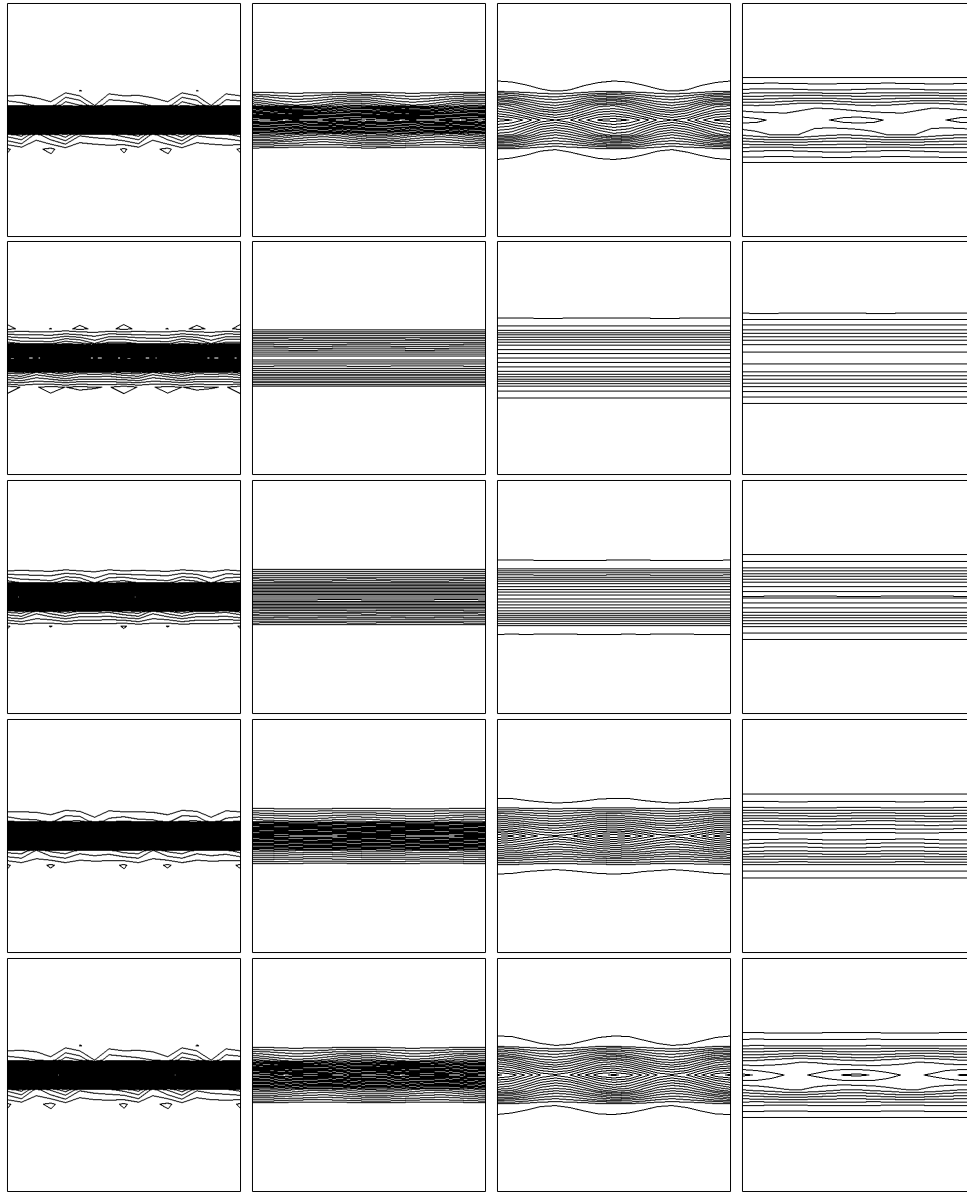


FIG. 5.6. *Three-dimensional mixing layer problem, vorticity at time units 10, 30, 60, 100 (left to right), Galerkin FEM, Smagorinsky model with $c_S = 0.005$, VMS with $L^H = P_0^{\text{disc}}$, VMS with $L^H = P_1^{\text{disc}}$, VMS with $L^H = P_2^{\text{disc}}$ (top to bottom).*

For $c_S = 0.005$, both solutions are almost the same in the whole time interval. The differences in the relative momentum thickness and the total kinetic energy of the VMS solutions obtained with $L^H = P_1^{\text{disc}}$ and $L^H = P_2^{\text{disc}}$ to the solution of the Navier–Stokes equations are presented in Figure 5.4. One can observe how small the differences in these two parameters are, but the plots of the vorticity show that the solutions differ considerably.

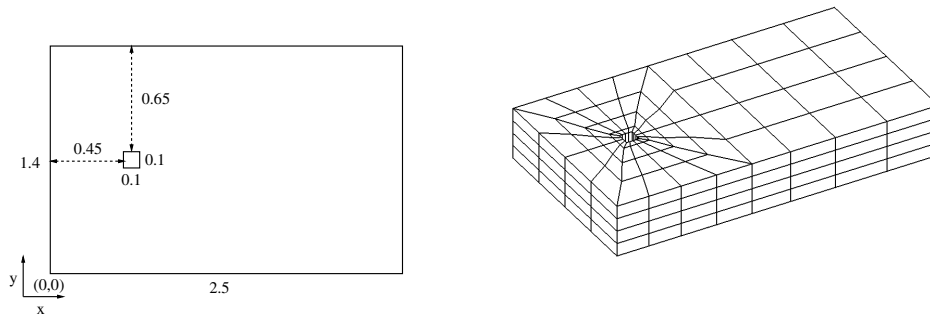


FIG. 5.7. Turbulent flow around a cylinder, the cross section of the domain (all length in m), and the initial grid; the height of the channel is $H = 0.4$ m.

5.3. A turbulent flow around a cylinder with square cross section. This example was defined by Rodi et al. [27]. The flow domain and the initial grid (level 0) consisting of hexahedra are given in Figure 5.7. The height of the channel is $H = 0.4$ m. The computations have been carried out on level 2, resulting in 522,720 velocity d.o.f. and 81,920 pressure d.o.f. The inflow is given by

$$\mathbf{u}(t, 0, y, z) = (1 + 0.04 * \text{rand}, 0, 0)^T,$$

where rand is a random number in $[-0.5, 0.5]$. The noise in the inflow serves to stimulate the turbulence. No-slip boundary conditions are prescribed at the column and outflow boundary conditions at $x = 2.5$. On all other boundaries, free slip conditions are used. The Reynolds number of the flow, based on the mean inflow $U_\infty = 1$ m/s, the length of the cylinder $D = 0.1$ m, and the viscosity $\nu = 1/220,000$ is $Re = 22,000$. There are no external forces acting on the flow. The Crank–Nicolson scheme was applied with equidistant time steps of length $\Delta t_n = 0.01$ and $\Delta t_n = 0.005$. Again, the Smagorinsky model (5.1) was used for the turbulent viscosity ν_T with $c_S = 0.005$ and $\delta = h_K$, where h_K is the diameter of the mesh cell K .

Characteristic values of the flow are the drag and the lift coefficient at the cylinder and the Strouhal number. The coefficients can be computed as volume integrals (e.g., see [20]),

$$c_d(t) = -\frac{2}{\rho D H U_\infty^2} [(\mathbf{u}_t, \mathbf{v}_d) + (\nu \nabla \mathbf{u}, \nabla \mathbf{v}_d) + b(\mathbf{u}, \mathbf{u}, \mathbf{v}_d) - (p, \nabla \cdot \mathbf{v}_d)]$$

for any function $\mathbf{v}_d \in (H^1(\Omega))^3$ with $(\mathbf{v}_d)|_S = (1, 0, 0)^T$; \mathbf{v}_d vanishes on all other boundaries and S is the boundary of the cylinder. The density of the fluid is in this example $\rho = 1$ kg/m³. Similarly, it holds that

$$c_l(t) = -\frac{2}{\rho D H U_\infty^2} [(\mathbf{u}_t, \mathbf{v}_l) + (\nu \nabla \mathbf{u}, \nabla \mathbf{v}_l) + b(\mathbf{u}, \mathbf{u}, \mathbf{v}_l) - (p, \nabla \cdot \mathbf{v}_l)]$$

for any function $\mathbf{v}_l \in (H^1(\Omega))^3$ with $(\mathbf{v}_l)|_S = (0, 1, 0)^T$ and \mathbf{v}_l vanishes on all other

TABLE 5.2
Results for the turbulent flow around a cylinder.

Method	Δt_n	\bar{c}_l	$c_{l,rms}$	\bar{c}_d	$c_{d,rms}$	St
Smagorinsky	0.01	0.001	1.295	2.507	0.103	0.152
VMS, $L^H = P_0^{\text{disc}}$	0.01	0.020	1.039	2.529	0.140	0.141
VMS, $L^H = P_1^{\text{disc}}$	0.01	-0.007	1.282	2.619	0.171	0.135
Smagorinsky	0.005	-0.001	1.190	2.482	0.079	0.152
VMS, $L^H = P_0^{\text{disc}}$	0.005	0.029	1.216	2.598	0.131	0.144
VMS, $L^H = P_1^{\text{disc}}$	0.005	0.017	1.276	2.614	0.151	0.132
ILLINOIS2		-0.02	1.40	2.52	0.27	0.13
UKAHY2		-0.04	1.15	2.30	0.14	0.13
experiments			0.7 - 1.4	1.9 - 2.1	0.1 - 0.2	0.132

boundaries. The actual choice of \mathbf{v}_d and \mathbf{v}_l in our computations is the same as in [22]. The Strouhal number is defined by $St = DU_\infty/T$, where T is a characteristic time scale (the average length of a period in this example).

In [27], the results obtained with more than a dozen codes are presented. These results include time averaged values \bar{c}_d , \bar{c}_l of the drag and lift coefficient, root mean squared values for c_d , c_l which are defined by

$$c_{d,rms} = \left(\sum_i (c_d(t_i) - \bar{c}_d)^2 \right)^{1/2}, \quad c_{l,rms} = \left(\sum_i (c_l(t_i) - \bar{c}_l)^2 \right)^{1/2},$$

where the summation covers all discrete times in the time interval for which \bar{c}_d , \bar{c}_l are computed, and the Strouhal number. However, the results of the different codes varied too much to define benchmark values. Some of the results from [27] are given, for comparison to our results, in Table 5.2. ILLINOIS2 is a code by Wang and Vanka, and UKAHY2 is a code by Pourquie, Breuer, and Rodi. In addition, values from experiments which were used in [27] also for comparison are given in Table 5.2.

The evolution of the lift coefficient for the Smagorinsky model, the VMS with $L^H = P_0^{\text{disc}}$, and the VMS with $L^H = P_1^{\text{disc}}$ is presented in Figure 5.8. The periodicity of the flow can be observed. The amplitudes of the lift coefficient vary much more for both VMS than for the Smagorinsky model. This shows that the flows computed with the VMS are more irregular (turbulent). The characteristic values of the flow, averaged over 10 periods, are presented in Table 5.2. It can be seen that they are in the range of the values computed with the engineering codes. The most reliable value with respect to the variation of the computational results in [27] is the Strouhal number. In our computations, this number is predicted the worst by the Smagorinsky model, clearly better by the VMS with $L^H = P_0^{\text{disc}}$, and by far the best by the VMS with $L^H = P_1^{\text{disc}}$. This is with respect to both the results obtained with the other codes and the experimental values. The different length of the periods computed with the different methods can be seen clearly in Figure 5.8. Altogether, using a VMS instead of the Smagorinsky model improves the computed flow in several aspects.

The computations were carried out at a computer with HP PA-RISC 8700 processors (3 GFlops peak). The assembling of the matrices for a VMS requires additional operations in comparison to the Smagorinsky model; see the description of our approach at the end of section 4. In this example, each assembling took approximately 111 s for the Smagorinsky model, 124 s for the VMS with P_0^{disc} , and 137 s for the

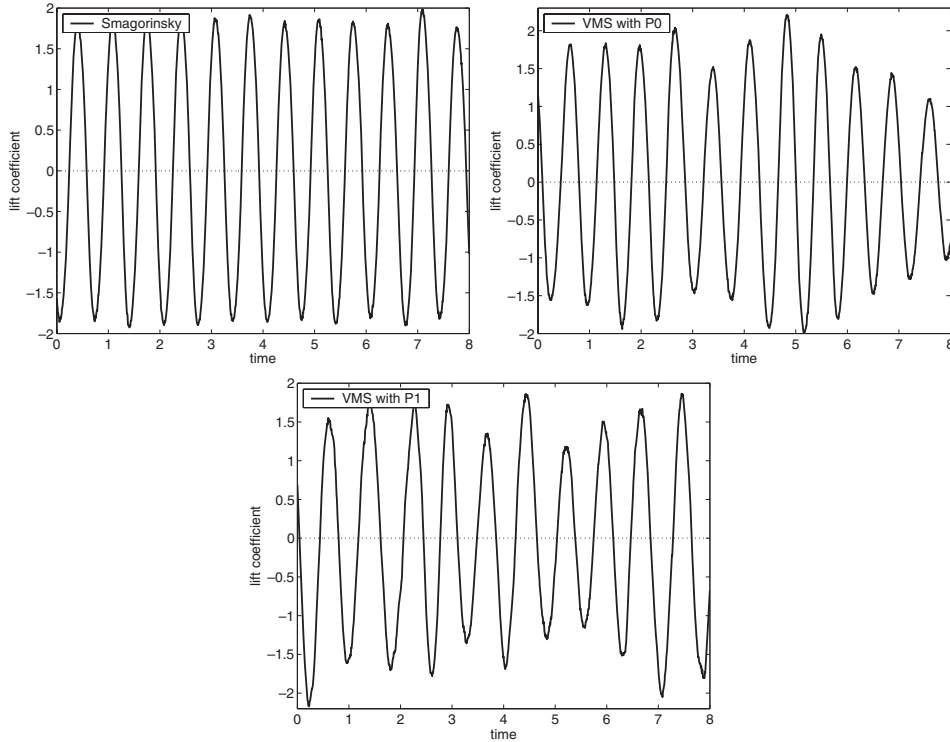


FIG. 5.8. Turbulent flow around a cylinder, evolution of the lift coefficient.

VMS with P_1^{disc} . Because of the noise in the inflow, the Euclidean norm of the residual was always rather large (more than $1e6$) at the beginning of each discrete time. The fixed point iteration for solving the nonlinearity was stopped after having reduced this norm below $1e-5$. In general, five iterations were necessary to reach this goal, independent of the method. Also the number of iterations for solving the linear saddle point problems was the same for all methods. The average time which was needed by the solver for one discrete time step was 490 s. It can be deduced from these observations that, at least in this example, the conditioning of the matrices is not much different for the Smagorinsky model and the VMS with P_k^{disc} , $k \in \{0, 1\}$. The only overhead of the VMS was indeed in the assembling of the matrices.

REFERENCES

- [1] R. ADAMS, *Sobolev Spaces*, Academic Press, New York, 1975.
- [2] L. BERSELLI, C. GRISANTI, AND V. JOHN, *On Commutation Errors in the Derivation of the Space Averaged Navier-Stokes Equations*, Preprint 12, Università di Pisa, Dipartimento di Matematica Applicata, 2004.
- [3] L. BERSELLI AND V. JOHN, *On the Comparison of a Commutation Error and the Reynolds Stress Tensor for Flows Obeying a Wall Law*, Preprint 18, Università di Pisa, Dipartimento di Matematica Applicata, 2004.
- [4] F. BREZZI, T. J. R. HUGHES, L. D. MARINI, A. RUSSO, AND E. SÜLI, *A priori error analysis of residual-free bubbles for advection-diffusion problems*, SIAM J. Numer. Anal., 36 (1999), pp. 1933–1948.

- [5] M. BRISTEAU, R. GLOWINSKI, AND J. PERIAUX, *Numerical methods for the Navier-Stokes equations: Applications to the simulation of compressible and incompressible viscous flows*, Comput. Phys. Rep., 6 (1987), pp. 73–187.
- [6] S. COLLIS, *Monitoring unresolved scales in multiscale turbulence modeling*, Phys. Fluids, 13 (2001), pp. 1800–1806.
- [7] P. COMTE, M. LESIEUR, AND E. LAMBALLAIS, *Large- and small-scale stirring of vorticity and a passive scalar in a 3-d temporal mixing layer*, Phys. Fluids A, 4 (1992), pp. 2761–2778.
- [8] T. DUBOIS, F. JAUBERTEAU, AND R. TEMAM, *Dynamic Multilevel Methods and the Numerical Simulation of Turbulence*, Cambridge University Press, Cambridge, UK, 1998.
- [9] A. DUNCA, V. JOHN, AND W. LAYTON, *The commutation error of the space averaged Navier-Stokes equations on a bounded domain*, in Contributions to Current Challenges in Mathematical Fluid Mechanics, Adv. Math. Fluid Mech. 3, G. P. Galdi, J. G. Heywood, and R. Rannacher, eds., Birkhäuser, Basel, 2004, pp. 53–78.
- [10] P. GRESHO AND R. SANI, *Incompressible Flow and the Finite Element Method*, John Wiley, Chichester, UK, 2000.
- [11] J.-L. GUERMOND, *Stabilization of Galerkin approximations of transport equations by subgrid modeling*, M2AN Math. Model. Numer. Anal., 33 (1999), pp. 1293–1316.
- [12] T. HUGHES, L. MAZZEI, AND K. JANSEN, *Large eddy simulation and the variational multiscale method*, Comput. Vis. Sci., 3 (2000), pp. 47–59.
- [13] T. HUGHES, L. MAZZEI, A. OBERAI, AND A. WRAY, *The multiscale formulation of large eddy simulation: Decay of homogeneous isotropic turbulence*, Phys. Fluids, 13 (2001), pp. 505–512.
- [14] T. HUGHES, A. OBERAI, AND L. MAZZEI, *Large eddy simulation of turbulent channel flows by the variational multiscale method*, Phys. Fluids, 13 (2001), pp. 1784–1799.
- [15] E. HYLIN AND J. McDONOUGH, *Chaotic small-scale velocity fields as prospective models for unresolved turbulence in an additive decomposition of the Navier-Stokes equations*, Int. J. Fluid Mech. Res., 26 (1999), pp. 539–567.
- [16] V. JOHN, *Higher order finite element methods and multigrid solvers in a benchmark problem for the 3D Navier-Stokes equations*, Internat. J. Numer. Methods Fluids, 40 (2002), pp. 775–798.
- [17] V. JOHN, *Slip with friction and penetration with resistance boundary conditions for the Navier-Stokes equations—numerical tests and aspects of the implementation*, J. Comput. Appl. Math., 147 (2002), pp. 287–300.
- [18] V. JOHN, *Large Eddy Simulation of Turbulent Incompressible Flows. Analytical and Numerical Results for a Class of LES Models*, Lect. Notes Comput. Sci. Eng. 34, Springer-Verlag, Berlin, Heidelberg, New York, 2004.
- [19] V. JOHN, *An assessment of two models for the subgrid scale tensor in the rational LES model*, J. Comput. Appl. Math., 173 (2005), pp. 57–80.
- [20] V. JOHN, *Reference values for drag and lift of a two-dimensional time dependent flow around a cylinder*, Internat. J. Numer. Methods Fluids, 44 (2004), pp. 777–788.
- [21] V. JOHN AND S. KAYA, *Finite Element Error Analysis of a Variational Multiscale Method for the Navier-Stokes Equations*, preprint, Otto-von-Guericke Universität Magdeburg, Fakultät für Mathematik, 2004.
- [22] V. JOHN AND G. MATTHIES, *Higher order finite element discretizations in a benchmark problem for incompressible flows*, Internat. J. Numer. Methods Fluids, 37 (2001), pp. 885–903.
- [23] V. JOHN AND G. MATTHIES, *MooNMD—a program package based on mapped finite element methods*, Comput. Vis. Sci., 6 (2004), pp. 163–170.
- [24] S. KAYA AND W. LAYTON, *Subgrid-Scale Eddy Viscosity Models are Variational Multiscale Methods*, Tech. report TR-MATH 03-05, University of Pittsburgh, 2003.
- [25] W. LAYTON, *A connection between subgrid scale eddy viscosity and mixed methods*, Appl. Math. Comput., 133 (2002), pp. 147–157.
- [26] Y. MADAY AND E. TADMOR, *Analysis of the spectral vanishing viscosity method for periodic conservation laws*, SIAM J. Numer. Anal., 26 (1989), pp. 854–870.
- [27] W. RODI, J. FERZIGER, M. BREUER, AND M. POURQUIÉ, *Status of large eddy simulation: Results of a workshop*, J. Fluids Eng., 119 (1997), pp. 248–262.
- [28] M. ROGERS AND R. MOSER, *Direct simulation of a self-similar turbulent flow*, Phys. Fluids, 6 (1994), pp. 903–923.
- [29] Y. SAAD, *A flexible inner-outer preconditioned GMRES algorithm*, SIAM J. Sci. Comput., 14 (1993), pp. 461–469.
- [30] P. SAGAUT, *Large Eddy Simulation for Incompressible Flows*, 2nd ed., Springer-Verlag, Berlin, Heidelberg, New York, 2003.
- [31] J. SMAGORINSKY, *General circulation experiments with the primitive equations*, Mon. Wea.

- Rev., 91 (1963), pp. 99–164.
- [32] S. TUREK, *Efficient Solvers for Incompressible Flow Problems: An Algorithmic and Computational Approach*, Lect. Notes Comput. Sci. Eng. 6, Springer-Verlag, Berlin, Heidelberg, New York, 1999.
- [33] B. VREMAN, B. GUERTS, AND H. KUERTEN, *Large-eddy simulation of turbulent mixing layer*, J. Fluid Mech., 339 (1997), pp. 357–390.